SUPPORTING INFORMATION

Detection of Low-Abundance Metabolites in Live Cells Using an RNA Integrator

Mingxu You[1,2,*], Jacob L. Litke[2], Rigumula Wu[1], and Samie R. Jaffrey[2,3,*]

[1] Department of Chemistry, University of Massachusetts, Amherst, MA 01003, USA.
[2] Department of Pharmacology, Weill Medical College, Cornell University, New York, NY 10065, USA
[3] Lead Contact

* Correspondence: srj2003@med.cornell.edu; mingxuyou@umass.edu

Table S1. Sequences for RNA integrators, Related to Figure 1 – 5, S1 – 4.

	RNA sensor sequence*
HHR-theophylline integrator	GUCUCCGCCUGAUGAGCCUUAGGAUAUGCUUCGGCAGAAGGACGUCGAAACGGUG AAAGCCGUA▼GCGGAGACGGUCGGGUCCAGAUAUUCGUAUCUGUCGAGUAGAGUG UGGGCUCCG
HHR-c-di-GMP integrator	GUCUCCGCCUGAUGAGAUGCACAGGGCAAACCAUUCGAAAGAGUGGGACGCAAAGC CUCCGGCCUAAACCAGAAGACAUGGUAGGUAGCGGGGUUACCAUCGAAACGGUGAA AGCCGUA▼GCGGAGACGGUCGGGUCCAGAUAUUCGUAUCUGUCGAGUAGAGUGUG GGCUCCG
HHR-cAMP integrator	GUCUCCGCCUGAUGAGCCUGUGGAAACAGACGUGGCACAUGACUACGUCGAAACGG UGAAAGCCGUA▼GCGGAGACGGUCGGGUCCAGAUAUUCGUAUCUGUCGAGUAGAG UGUGGGCUCCG
HHR-theophylline	GGGCGACCCUGAUGAGCCUUAGGAUAUGCUUCGGCAGAAGGACGUCGAAACGGUG AAAGCCGUA▼GGUUGCCC
Twister-theophylline integrator	GUCUCCGCU▼AACACUGCCCCUUAGGAUAUGCUUCGGCAGAAGGACGUGCCGGUCC CAAGCCCGGAUAAAAGUGGAGGGGCGGAGACGGUCGGGUCCAGAUAUUCGUAUCU GUCGAGUAGAGUGUGGGCUCCG
Pistol-theophylline integrator	GUCUCCGCAAAAAAAAAAGGACUCGACUAAGCGAGUAUAAACAGGCAUUAGGCUUAG AGCGUCCUUAGGAUAUGCUUCGGCAGAAGGACGUGG▼UUGCAAAAAAAAAAAGCGG AGACGGUCGGGUCCAGAUAUUCGUAUCUGUCGAGUAGAGUGUGGGCUCCG
Varkud satellite-theophylline integrator	GUCUCCGCAAAUGCG▼AAGGGCGUCGUCGCCCCGAGCGGUAGUAAGCAGGGAACU CACCUCCAAUUUCCCUUAGGAUAUGCUUCGGCAGAAGGACGUGAAAUUGUCGUAGC AGUUGACUACUGUUAUGUGAUUGGUAGAGGCUAAGUGACGGUAUUGGCGUAAGUC AGUAUUGCAGCACAGCACAAGCCCGCUUGCGAGAAUGCGGAGACGGUCGGGUCCA GAUAUUCGUAUCUGUCGAGUAGAGUGUGGGCUCCG
Twister sister-theophylline integrator	GUCUCCGCGCAAGGCCGACGGCAUCCGCCGCCGCUGGUGCAAGUCCAGCCGCCUU AGGAUAUGCUUCGGCAGAAGGACGUCGGGCGCUC▼AUGCGGAGACGGUCGGGUCC AGAUAUUCGUAUCUGUCGAGUAGAGUGUGGGCUCCG
Hairpin-theophylline integrator	GUCUCCGCAGAGAAGUCAACCAGAGAAACACACCCUUAGGAUAUGCUUCGGCAGAA GGACGUGUGGUAUAUUACCUGGUACUGACA▼GUCCUGCGGAGACGGUCGGGUCCA GAUAUUCGUAUCUGUCGAGUAGAGUGUGGGCUCCG
Extended HHR-theophylline integrator	GUCUCCGCGUACAUCCAGCUGAUGAGUCCCAAAUAGGACGAAACCCAUACCAGCCG AAAGGCCCUUGGCAGGGCGUC▼CUGGAUUCCAGGCGGAGACGGUCGGGUCCAGAU AUUCGUAUCUGUCGAGUAGAGUGUGGGCUCCG
Extended HHR-c-di-GMP integrator	GUCUCCGCGUACAUCCAGCUGAUGAGUCCCAAAUAGGACGAAAAUGCACAGGGCAA ACCAUUCGAAAGAGUGGGACGCAAAGCCUCCGGCCUAAACCAGAAGACAUGGUAGG UAGCGGGGUUACCAUUC▼CUGGAUUCCAGGCGGAGACGGUCGGGUCCAGAUAUUC GUAUCUGUCGAGUAGAGUGUGGGCUCCG
Extended HHR-TPP integrator	GUCUCCGCGUACAUCCAGCUGAUGAGUCCCAAAUAGGACGAAACUAAAGGGAUGCG ACCGUAAUAGGUCUAGUCCACUAUGCCCAUAAAGAGUCGGAAGUGCGUCUUCCCGU GGGGCUUCGUC▼CUGGAUUCCAGGCGGAGACGGUCGGGUCCAGAUAUUCGUAUCU GUCGAGUAGAGUGUGGGCUCCG
Extended HHR-Broccoli	GUCUCCGCGUACAUCCAGCUGAUGAGUCCCAAAUAGGACGAAACGGCGAAAGCCGU C▼CUGGAUUCCAGGCGGAGACGGUCGGGUCCAGAUAUUCGUAUCUGUCGAGUAGA GUGUGGGCUCCG

* The blue sequence indicates the aptamer domain for target binding, the green sequence indicates the Broccoli sequence, and the black sequence indicates the ribozyme part. ▼ indicates the self-cleavage site of each sensor. Highlighted green, yellow, and grey region indicate the A, A', and A'' sequence, respectively.

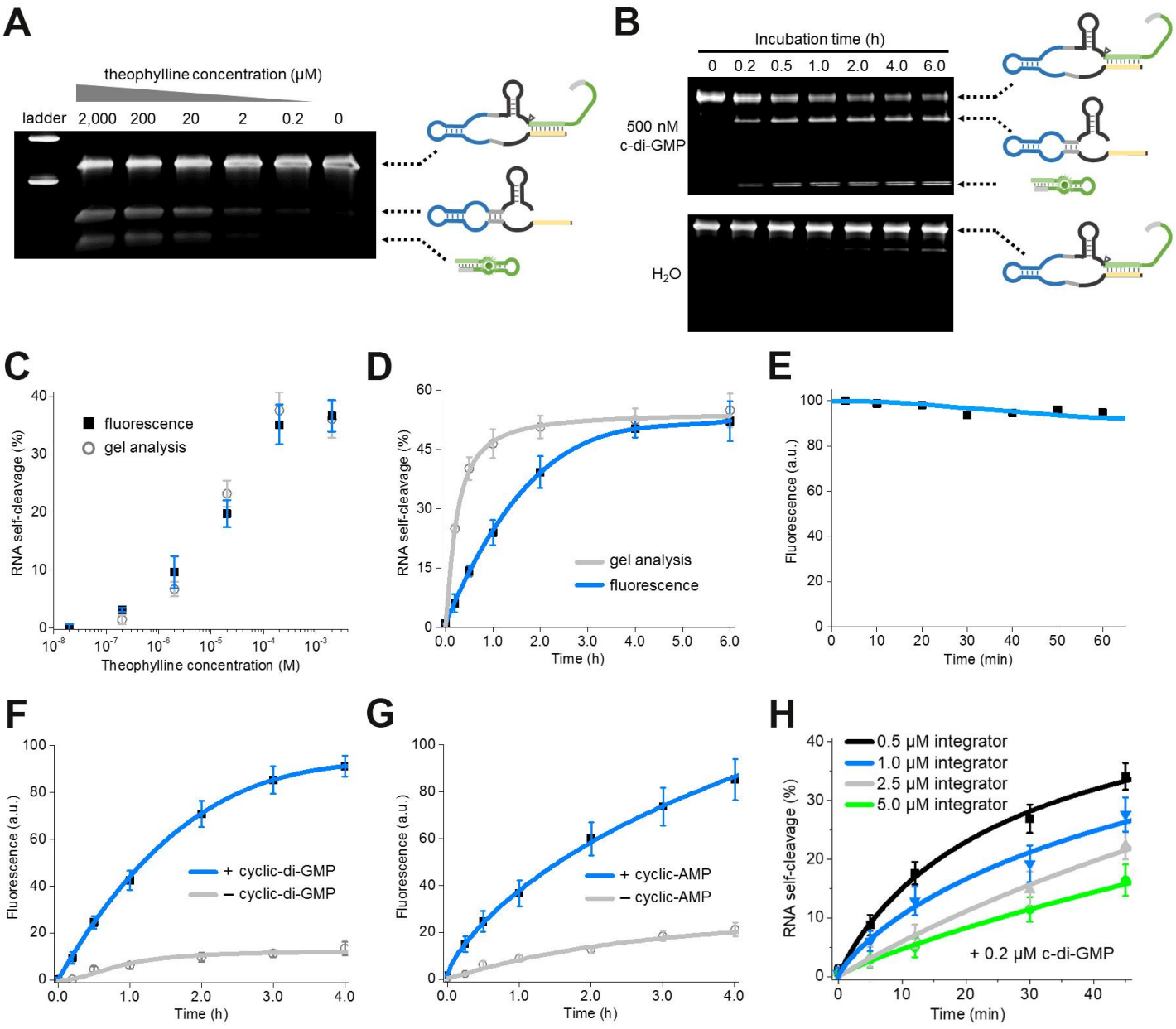

Figure S1. *In vitro* properties of the RNA integrator that is based on the minimal conserved domain of HHR, Related to Figure 2 and 4.

(A) Theophylline-induced self-cleavage of the RNA integrator. 0.2 – 2,000 μM theophylline was incubated with 1 μM theophylline-targeting RNA integrator for 2 h. Then, the RNA was resolved by

a 6% urea-PAGE gel followed by staining for 30 min with SYBR Gold dye (Life Technologies) diluted 1/10,000 in TBE buffer.

(B) Kinetics of c-di-GMP-induced self-cleavage of the RNA integrator. 500 nM c-di-GMP or water was added to a solution of 1 μM c-di-GMP-targeting RNA integrator for 0 – 6 h. Then, the RNA was resolved by a 6% urea-PAGE gel followed by staining for 30 min with SYBR Gold dye (Life Technologies) diluted 1/10,000 in TBE buffer. Minimal cleavage was observed without the addition of c-di-GMP.

(C) The direct correlation between the percentage of RNA cleavage and the fluorescence enhancement of the RNA integrator. The fold of fluorescence enhancement 2 h after the addition of 0.2 – 2,000 μM theophylline into 1 μM RNA sensor was plotted against the concentration of theophylline. Gel electrophoresis as shown in Figure S1A was used to measure the percentage of the self-cleavage of RNA integrator. Gel band intensities were quantified in Image Lab 5.0 software (Bio-Rad).

(D) The relative kinetics of RNA cleavage and fluorescence enhancement of the RNA integrator. The kinetics of fluorescence enhancement of 1 μM c-di-GMP-targeting RNA sensor after the addition of 500 nM c-di-GMP was plotted against the incubation time. Gel electrophoresis as shown in Figure S1C was used to measure the percentage of self-cleavage of the RNA integrator. Gel band intensities were quantified in Image Lab 5.0 software (Bio-Rad).

(E) Measurement of the RNA integrator fluorescence after removing the target at 0 min. 1 μM theophylline-targeting RNA integrator was incubated with 200 μM theophylline for 1 h, and then the theophylline was removed by a rapid gel filtration step to separate the RNA from the small molecule. More than 95% of the fluorescence signal was retained during the measurement period.

(F) Measurement of the rate of RNA integrator activation. As can be seen, addition of 2 μM c-di-GMP led to rapid signal acquisition (blue), with more than half of the total fluorescence signal appearing in ~69 min. Shown are mean and SEM values of three independent replicates.

(G) Measurement of the rate of RNA integrator activation. As can be seen, addition of 1 mM cAMP led to rapid signal acquisition (blue), with more than half of the total fluorescence signal appearing in ~85 min. Shown are mean and SEM values of three independent replicates.

(H) Kinetics of c-di-GMP-induced initial self-cleavage of the RNA integrator, which can be used to determine the turnover rate of c-di-GMP during the activation of the RNA integrator. Here, 200 nM c-di-GMP was added to a solution of 0.5 – 5 μM c-di-GMP-targeting RNA integrator. After different incubation time, the cleavage efficiency of RNAs was resolved in a 6% urea-PAGE gel. The turnover number, k'_{cat}, can then be calculated based on an Eadie-Hofstee diagram (Hofstee, 1959) by considering c-di-GMP as the catalyst and the RNA integrator as the substrate.

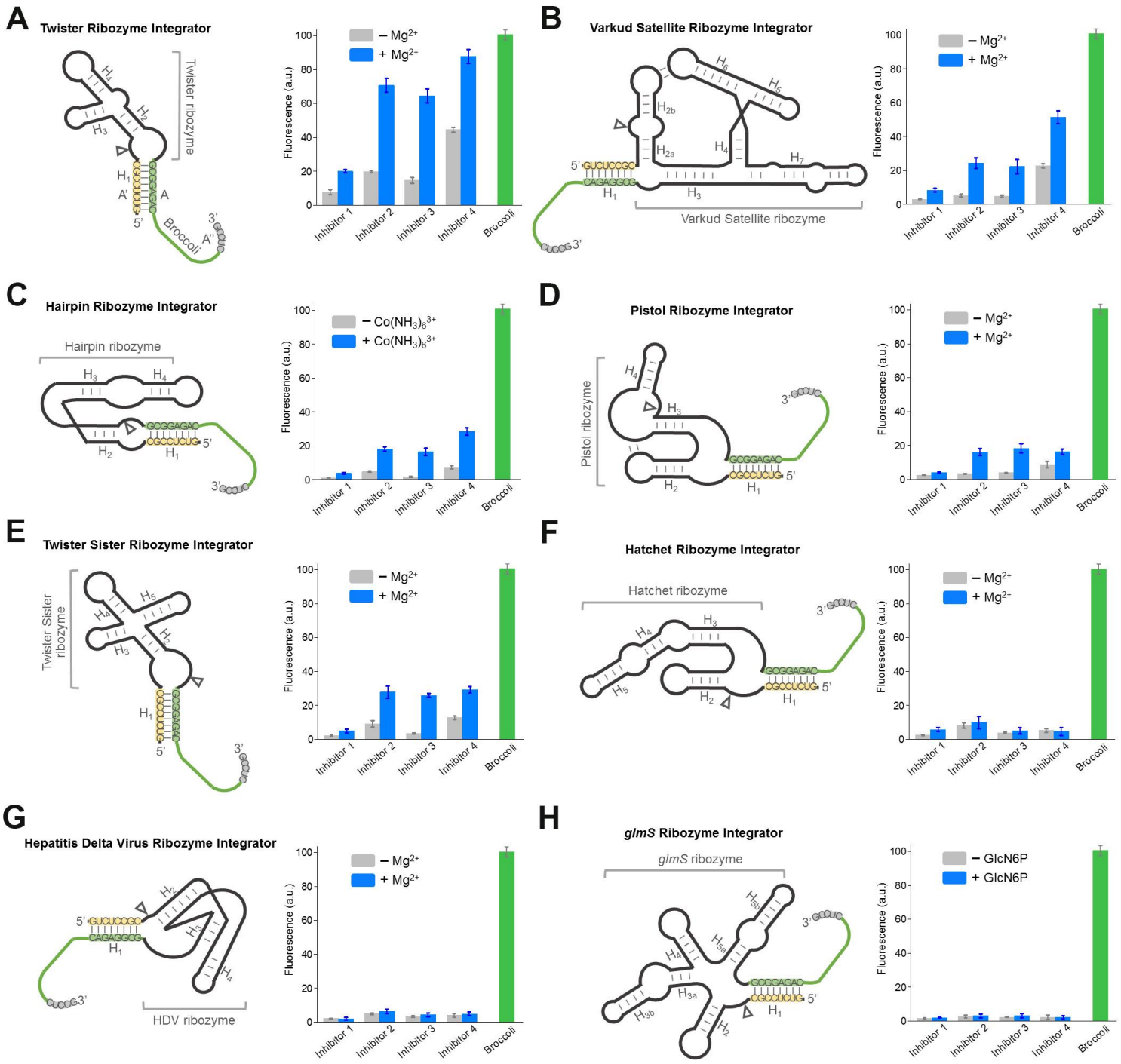

Figure S2. Secondary structure and performance of RNA integrators that utilize diverse naturally occurring *cis*-acting ribozymes, Related to Figure 3.

(A) Secondary structure and design of the twister ribozyme integrator. The integrator is generated by swapping Broccoli-inhibitor A-A'-A'' complex (green-yellow-grey) into the H_1 domain of the twister ribozyme. Shown are the sequences from the Inhibitor 3 complex. Performance of the

RNA integrator was measured 2 h after the addition of 10 mM Mg^{2+}. Shown are mean and SEM values of three independent replicates.

(B) Secondary structure and design of the Varkud satellite ribozyme integrator. The integrator is generated by swapping Broccoli-inhibitor A-A'-A'' complex (green-yellow-grey) into the H_1 domain of the Varkud satellite ribozyme. Shown are the sequences from the Inhibitor 3 complex. Performance of the RNA integrator was measured 2 h after the addition of 10 mM Mg^{2+}. Shown are mean and SEM values of three independent replicates.

(C) Secondary structure and design of the hairpin ribozyme integrator. The integrator is generated by swapping Broccoli-inhibitor A-A'-A'' complex (green-yellow-grey) into the H_1 domain of the hairpin ribozyme. Shown are the sequences from the Inhibitor 3 complex. Performance of the RNA integrator was measured 2 h after the addition of 10 mM $Co(NH_3)_6^{3+}$. Shown are mean and SEM values of three independent replicates.

(D) Secondary structure and design of the pistol ribozyme integrator. The integrator is generated by swapping Broccoli-inhibitor A-A'-A'' complex (green-yellow-grey) into the H_1 domain of the pistol ribozyme. Shown are the sequences from the Inhibitor 3 complex. Performance of the RNA integrator was measured 2 h after the addition of 20 mM Mg^{2+}. Shown are mean and SEM values of three independent replicates.

(E) Secondary structure and design of the twister sister ribozyme integrator. The ribozyme integrator is generated by swapping Broccoli-inhibitor A-A'-A'' complex (green-yellow-grey) into the H_1 domain of the twister sister ribozyme. Shown are the sequences from the Inhibitor 3 complex. Performance of the RNA integrator was measured 2 h after the addition of 10 mM Mg^{2+}. Shown are mean and SEM values of three independent replicates.

(F) Secondary structure and design of the hatchet ribozyme integrator. The integrator is generated by swapping Broccoli-inhibitor A-A'-A'' complex (green-yellow-grey) into the H_1 domain of the hatchet ribozyme. Shown are the sequences from the Inhibitor 3 complex. Performance of the RNA integrator was measured 2 h after the addition of 10 mM Mg^{2+}. Shown are mean and SEM values of three independent replicates.

(G) Secondary structure and design of the HDV ribozyme integrator. The integrator is generated by swapping Broccoli-inhibitor A-A'-A'' complex (green-yellow-grey) into the H_1 domain of the HDV ribozyme. Shown are the sequences from the Inhibitor 3 complex. Performance of the RNA integrator was measured 2 h after the addition of 10 mM Mg^{2+}. Shown are mean and SEM values of three independent replicates.

(H) Secondary structure and design of the *glmS* ribozyme integrator. The integrator is generated by swapping Broccoli-inhibitor A-A'-A'' complex (green-yellow-grey) into the H_1 domain of the *glmS* ribozyme. Shown are the sequences from the Inhibitor 3 complex. Performance of the RNA integrator was measured 2 h after the addition of 5 mM glucosamine-6-phosphate. Shown are mean and SEM values of three independent replicates.

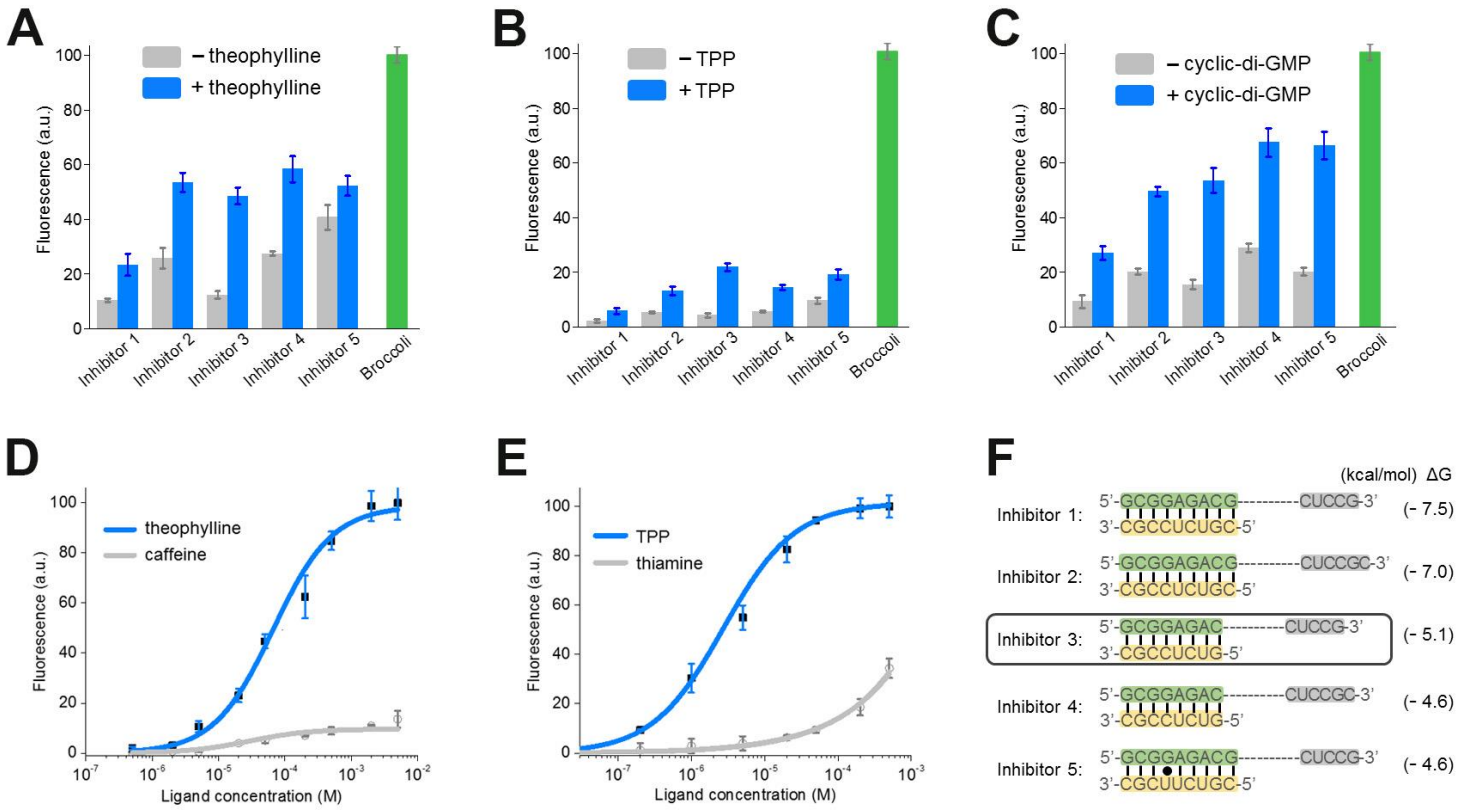

Figure S3. *In vitro* properties of the RNA integrator that is based on the pseudoknot-containing HHR, Related to Figure 5.

(A) Optimization of theophylline-targeting RNA integrators. An aptamer domain that can selectively bind theophylline (Jenison et al., 1994) was connected into the H_3 stem of extended HHR. Shown are mean and SEM values of three independent replicates. The optimal sensor (Inhibitor 3) displayed a 3.9-fold increase in fluorescence signal 2 h after the addition of 200 µM theophylline.

(B) Optimization of TPP-targeting RNA integrators. An aptamer domain that can selectively bind TPP (Winkler et al., 2002) was connected into the H_3 stem of extended HHR. Shown are mean and SEM values of three independent replicates. The optimal sensor (Inhibitor 3) displayed a 5.4-fold increase in fluorescence signal 2 h after the addition of 100 µM TPP.

(C) Optimization of cyclic di-guanylate-targeting RNA integrators. An aptamer domain that can selectively bind cyclic di-guanylate (Sudarsan et al., 2008) was connected into the H_3 stem of extended HHR. Shown are mean and SEM values of three independent replicates. The optimal sensor (Inhibitor 3) displayed a 3.5-fold increase in fluorescence signal 2 h after the addition of 2 µM cyclic di-guanylate.

(D) Dose-response curve for fluorescence activation of the theophylline-extended integrator by either theophylline or caffeine, two molecules that differ by a single methyl group. Half-maximal fluorescence is reached at 65 µM theophylline (blue). Shown are mean and SEM values of three

independent replicates. The theophylline integrator is highly specific for theophylline, which is consistent with the known binding specificity of the aptamer (Jenison et al., 1994).

(E) Dose-response curve for fluorescence activation of the TPP-extended integrator by either TPP or thiamine. Half-maximal fluorescence is reached at 2.7 μM TPP (blue). Shown are mean and SEM values of three independent replicates. The theophylline integrator is highly specific for TPP, which is consistent with the known binding specificity of the aptamer (Winkler et al., 2002).

(F) Sequences of the five tested Broccoli-inhibitor complexes (Inhibitor 1 – 5) in Figure S3A-C. In each case, an 8- or 9-nucleotide long A' inhibitor strand (yellow) forms a duplex with the A strand region (green) in Broccoli. After the target-induced cleavage of HHR, the A strands can instead form duplexes with an A" sequence (grey), which is a component of Broccoli stem required for the fluorescence activation. The optimal sensor (Inhibitor 3) contained eight and five Watson-Crick base pairs, respectively, in the A-A' and A-A'' duplex. The predicted Gibbs free energy change (ΔG) during hybridization switch between the A-A' duplex and A-A'' duplex was calculated using mfold online software (Zuker, 2003).

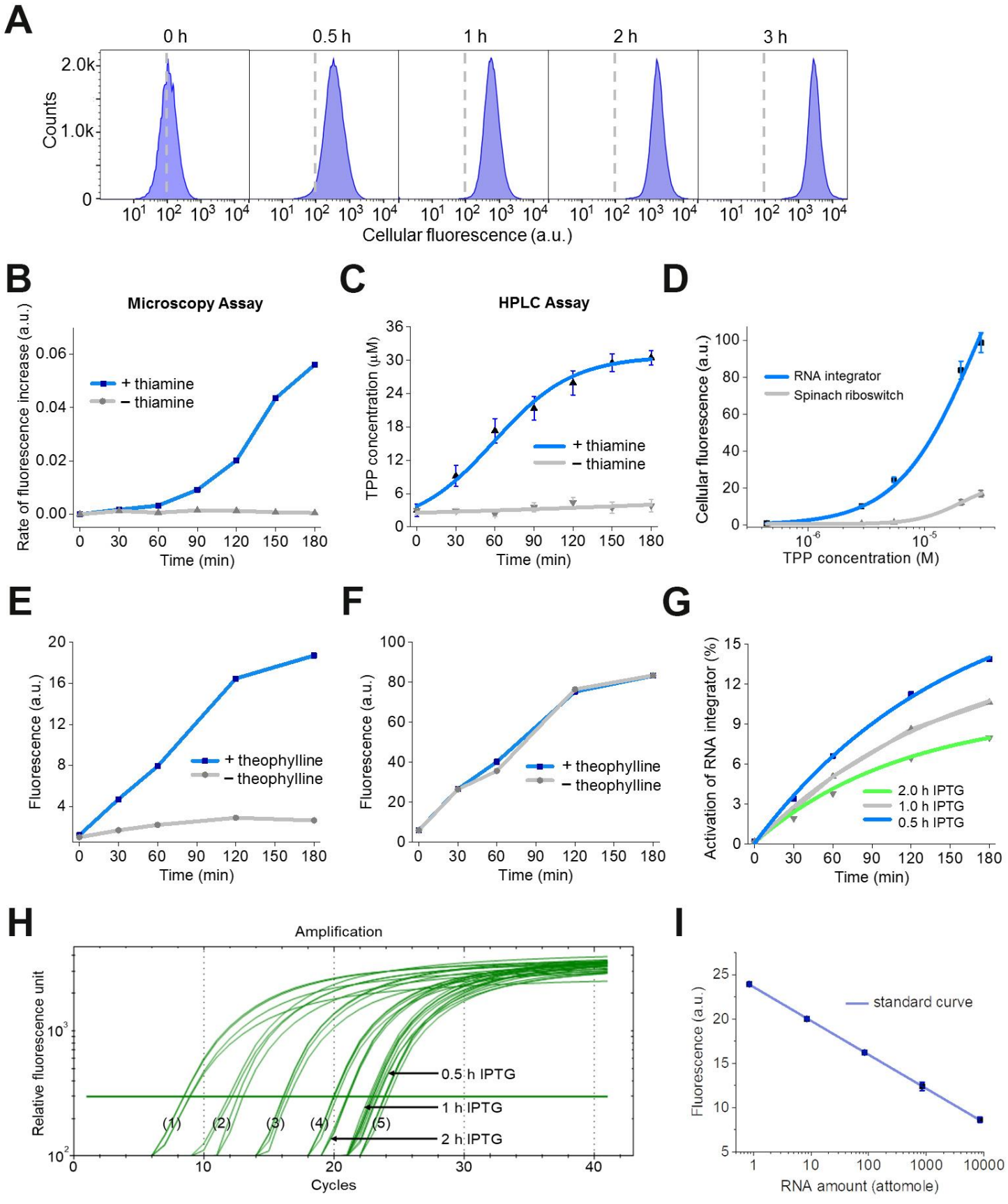
A
0 h
0.5 h
1 h
2 h
3 h
Counts
2.0k
1.0k
0
Cellular fluorescence (a.u.)
B
Microscopy Assay
Rate of fluorescence increase (a.u.)
+ thiamine
– thiamine
Time (min)
C
HPLC Assay
TPP concentration (μM)
+ thiamine
– thiamine
Time (min)
D
Cellular fluorescence (a.u.)
RNA integrator
Spinach riboswitch
TPP concentration (M)
E
Fluorescence (a.u.)
+ theophylline
– theophylline
Time (min)
F
Fluorescence (a.u.)
+ theophylline
– theophylline
Time (min)
G
Activation of RNA integrator (%)
2.0 h IPTG
1.0 h IPTG
0.5 h IPTG
Time (min)
H
Amplification
Relative fluorescence unit
0.5 h IPTG
1 h IPTG
2 h IPTG
(1)
(2)
(3)
(4)
(5)
Cycles
I
Fluorescence (a.u.)
standard curve
RNA amount (attomole)

Figure S4. RNA integrator measures metabolite concentrations in living cells, Related to Figure 5.

(A) Kinetics of TPP biosynthesis in *E. coli*. Cells expressing the TPP integrator were briefly cultured in thiamine-free media for 2 h, and then following addition of 10 μM thiamine, fluorescence signal from 100,000 individual cells was quantified every 30 min for 3 h by flow cytometry. A time-dependent increase in the mean cellular fluorescence was observed.

(B) Cellular fluorescence activation of the TPP integrator. As shown in Figure S4A, the TPP integrator fluorescence was measured after adding 10 μM thiamine (blue) or vehicle alone (grey) every 30 min for 3 h with a flow cytometry. The mean cellular fluorescence from 100,000 individual cells was plotted against the incubation time. A time-dependent increase in the mean cellular fluorescence was observed at each time point.

(C) Cellular accumulation of TPP as measured in an HPLC assay. Cells expressing the TPP integrator were treated identically as shown in Figure S4A, B. These cells were briefly cultured in thiamine-free media for 2 h, and then 10 μM thiamine (blue) or vehicle alone (grey) was added. Cells were lysed at different time points to measure total TPP levels using an HPLC assay. Error bar represents the SEM from three experimental replicates.

(D) Dose-response curve for cellular fluorescence activation of the TPP integrator and Spinach riboswitch sensors. The intracellular TPP concentrations were measured in an HPLC assay. At each concentration, shown are the mean and SEM cellular fluorescence from 100,000 individual cells as measured by flow cytometry after 3 h incubation with 0 – 10 μM thiamine. Cellular fluorescence level 3h after culturing in thiamine-free 300 μg/ml adenosine media was used as the background. Adenosine can inhibit the synthesis of thiazole phosphate, a TPP precursor in the de novo TPP biosynthesis pathway (Kawasi et al., 1969).

(E) Cellular fluorescence activation of the theophylline integrator. The theophylline integrator fluorescence was measured after adding 200 μM theophylline (blue) or vehicle alone (grey) for 3 h with a flow cytometry. The mean cellular fluorescence from 5,000 individual cells was plotted against the incubation time. A time-dependent increase in the theophylline-induced mean cellular fluorescence was observed at each time point, while in the absence of theophylline, some minimal background fluorescence was observed.

(F) Cellular fluorescence activation of the HHR-Broccoli construct. These HHR-Broccoli can be spontaneously activated to induce Broccoli fluorescence. The HHR-Broccoli fluorescence was measured after adding 200 μM theophylline (blue) or vehicle alone (grey) for 3 h with a flow cytometry. The mean cellular fluorescence from 5,000 individual cells was plotted against the incubation time. A time-dependent increase in the mean cellular fluorescence was observed at each time point independent of theophylline.

(G) Kinetics of theophylline-induced cellular fluorescence activation of the RNA integrator. Cells expressing the theophylline integrator were induced for 0.5 – 2 hours with 1 mM IPTG at 37°C. The integrator fluorescence was measured after adding 2 μM theophylline for 3 h with a flow cytometry. The mean cellular fluorescence from 5,000 individual cells were plotted against the

incubation time. The turnover number, k'_{cat}, 0.018 min^{-1}, can then be calculated based on an Eadie-Hofstee diagram (Hofstee, 1959) by considering theophylline as the catalyst and the RNA integrator as the substrate.

(H) Quantifying the cellular level of the RNA integrator with real-time PCR. The real-time fluorescence units were plotted against standard RNA samples of (1) 8,500, (2) 850, (3) 85, (4) 8.5, and (5) 0.85 attomoles with four replicates at each concentration. In the same experiment, the relative fluorescence units were used to determine the amount of the RNA integrator from cells expressing the theophylline integrator after induction for 0.5 – 2 hours with 1 mM IPTG at 37°C.

(I) A standard curve to correlate the real-time PCR data with the RNA amount. The curve was based on data from Figure S4H with standard RNA samples of 0.85 – 8,500 attomoles. This standard curve was further used to calculate the intracellular amount of the RNA integrator.